Self-Driven Magnetic Fluid Cooling for Power Devices Utilizing Permanent Magnet

Masataka Anazawa
Dept. of Electrical, Electronics, and Information Engineering
Nagaoka University of Technology
Niigata, Japan
s233091@stn.nagaokaut.ac.jp
Masaaki Baba
Dept. Mechanical Engineering.
Nagaoka University of Technology
Niigata, Japan
m-baba@mech.nagaokaut.ac.jp

Masato Suzuki
Dept. Mechanical Engineering.
Nagaoka University of Technology
Niigata, Japan
s223037@stn.nagaokaut.ac.jp
Keisuke Kusaka
Dept. of Electrical, Electronics, and Information Engineering
Nagaoka University of Technology
Niigata, Japan
kusaka@vos.nagaokaut.ac.jp

Abstract—In photovoltaic power conditioning systems (PCSs), the lifespan of the inverter is shorter than that of the solar panels, which is a significant factor limiting the overall system duration. One of the causes responsible for inverter failure is a malfunction of the cooling system. This is often due to contamination or wear of the mechanical components in the cooling mechanism. To address this issue, a passive cooling system using temperaturesensitive magnetic fluid (TSMF) has been developed. TSMF has the characteristic of exhibiting changes in magnetic properties near room temperature, and this property is utilized to cool semiconductor power devices. However, the effect of the magnet position required for TSMF drive on the cooling capacity of the TSMF remains unclear. This paper investigates the relationship between magnetic field, driving force, and cooling performance. Using a dedicated measurement device, it was confirmed that the driving force increases as the magnetic source is moved closer to the high-temperature region. Furthermore, measurements of heat transfer performance test confirmed that the suggested placement of the magnetic source in this paper helps increase the temperature gradient, which in turn leads to an enhancement of heat transfer capability, achieving a thermal resistance reduction of 1.4 °C/W.

Keywords— Magnetic fluid; Passive cooling system; Heat transfer; Magnetic power.

I. Introduction

In the past decade, the adoption and transition to renewable energy have accelerated to address the ongoing issue of greenhouse gas emissions. Particularly, solar power generation has witnessed rapid growth in operation, with cumulative installed capacity of PV systems exceeding 1.6 TW as of early 2024. Solar PV system generates 2,137 TWh annually, accounting for 8.3% of global electricity demand, and its deployment continues to expand worldwide [1–2].

The lifespan of a PV system is mainly determined by its inverter. Since the inverter's lifespan is only half that of the PV system, it poses a significant reliability problem [3–5]. There are numerous reasons for inverter failures, one of which is

damage to power semiconductors due to thermal cycling [6–7]. To extend the life duration of an inverter, and mitigate thermal issues, a large-capacity cooling device with optimized heat dispersion for power modules is necessary [7–9]. Such a cooling device achieves efficient thermal dissipation with forced air cooling using mechanical components.

However, cooling devices with mechanical components tend to have a short lifespan [10]. Since these devices are the second most common cause of power supply failures [11], their use leads to a decrease in system reliability. For residential power conditioners operated over a long period of time, highly reliable thermal management using non-mechanical cooling device has become more demanding. In contribution to the development of heat transport devices that do not use mechanical components, research on vapor chambers and heat pipes are still progressing [12–13], yet those solutions are heavily affected by gravity and various restrictions on their installation orientation. To resolve this, a non-mechanical, orientation-independent thermal transport device has been proposed [14–16] using the temperature characteristics and magnetic force of a magnetic fluid.

Magnetic fluid cooling systems operate without mechanical components, thereby addressing issues related to the limited lifespan of conventional cooling devices. When applied to the thermal management of power electronic devices, this technology has the potential to enhance the reliability of photovoltaic (PV) systems. However, several fundamental aspects remain unclear, including the mechanisms by which the external magnetic field generates a driving force and the heat transfer capabilities of the system. Currently, a comprehensive design methodology has not yet been established.

This paper describes the development of a device for measuring the driving force of a magnetic fluid, aiming to clarify the relationship between the fluid temperature and its driving force for the design of a magnetic fluid heat transfer system. The device was used to obtain data on the driving force characteristics of the magnetic fluid as a function of temperature and magnetic field strength, as well as its

dependence on the position of the magnet. Using this driving force data, a heat transfer device capable of circulating the magnetic fluid was developed, and it was found that the heat transfer performance varies depending on the magnet position.

II. TSMF DRIVING PRINCIPLE

A. Temperature-Sensitive Magnetic Fluid (TSMF)

In this study, temperature-sensitive magnetic fluid (TSMF) is used as the fluid medium. Magnetic fluid is a liquid in which microscopic magnetic particles are dispersed in a carrier fluid, possessing properties of both liquids and magnetic materials. TSMF, in addition to having similar properties to conventional fluids. exhibits a significant magnetic decrease magnetization with increasing temperature near room temperature [14–16]. In this study, TC3030S material (Ferrotec Co.) is used. This fluid has the physical properties shown in Table 1 and the temperature dependence shown in Fig. 1. Fig. 1 shows the change in magnetization with temperature, using 25°C as the reference temperature. The magnetization M [A/m] at each temperature is normalized by dividing it by the maximum magnetization value M_s [A/m]. As shown in Fig. 1, saturation magnetization decreases with increasing temperature. As a result, when TSMF is heated in a magnetic field, its magnetic attraction also decreases.

B. Driving principle

Fig. 1 shows the temperature-magnetization characteristics of the temperature-sensitive magnetic fluid. Fig. 2 shows an image of driving force generation. A hot section and a cold section are formed in a flow path filled with TSMF. A magnet is placed at the temperature boundary, and this arrangement generates a steep magnetic field gradient at the temperature boundary. With this arrangement, TSMF is attracted from both sides to the temperature boundary with the large magnetic field gradient. This force is called magnetic volume force F [N/m³] [14–16]. The magnetic volume force is determined by the product of the gradient of the magnetic field H [A/m] and the magnetization M [A/m].

$$F = \mu_0(M \cdot \nabla H)$$
(1)

In TSMF, the decrease in magnetization with increasing temperature on the high-temperature side creates a magnetic non-equilibrium between the low-temperature and high-temperature regions. This temperature-dependent magnetization change also results in a non-equilibrium in the magnetic volume force. Consequently, a driving force, ΔF , is generated from the low-temperature to the high-temperature side due to the difference in the magnetic volume force.

$$\Delta F = F_{Tlow} - F_{Thieh} \qquad (2)$$

III. DRIVING FORCE ANALYSIS

A driving force is generated by applying a magnetic force and a temperature difference to the magnetic fluid. The parameters that are important for understanding the characteristics and design of the driving force are verified and reported below.

Table 1 Physical properties of TC3030S.

Properties	Symbol	Value
Dispersion medium		Synthetic hydrocarbons
Saturation magnetic flux density @25°C	B_{sat}	30.0 mT
Density @25°C	ρ	$1.17 \times 10^3 \text{ kg/m}^3$
Thermal conductivity @22°C	λ	0.143 W/(m·K)
Specific heat	C_p	1420 J/(kg•K)

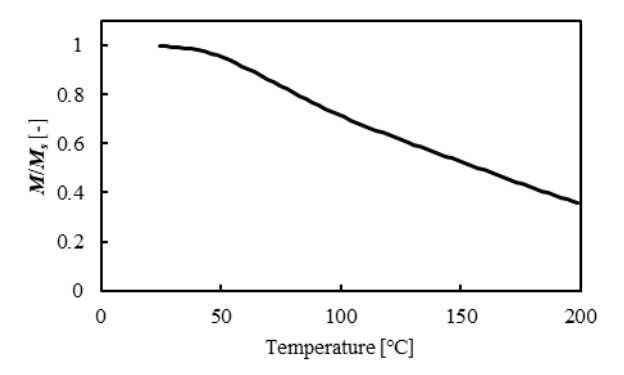


Fig. 1. Temperature-magnetization characteristics of TC3030S.

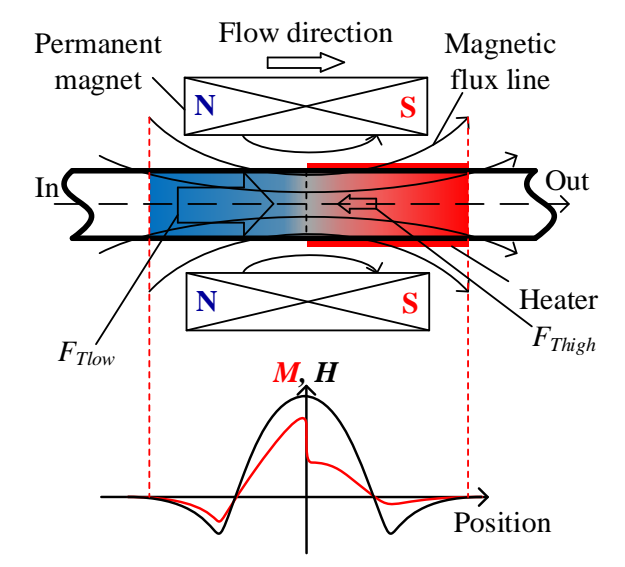


Fig. 2. Magnetic fluid driving principle.

A. Driving Force Measuring Instrument

A driving force measuring instrument capable of measuring the driving force as pressure was developed and illustrated with a schematic diagram in Fig. 3. This device measures the driving force generated in the TSMF by measuring the height of the liquid column. The device is configured as a U-shaped tube filled with TSMF and is adjusted to be parallel to the ground so that the heights of the liquid columns on the left and right are equal in the initial state. By applying a temperature

difference to both ends of the magnet, the TSMF obtains a driving force from the cooling side to the heating side. As a result, the liquid column on the cooling side descends and the liquid column on the heating side rises, creating a difference in the liquid column height on the left and right. If the density of the liquid is known, the pressure P [Pa] can be calculated by the product of the fluid density ρ [kg/m³], gravitational acceleration g [m/s²], and the liquid column difference Δh [m] [17]. Here, the thermal expansion coefficient of the TSMF liquid is ignored as it is sufficiently small.

$$\mathbf{P} = \rho \mathbf{g} \Delta h$$
(3)

Fig. 3 shows the configuration diagram of the pressure measuring instrument. Fig. 4 shows the actual pressure measuring instrument. As shown in Fig. 4, this device consists of a U-shaped tube, composed of a copper pipe and a glass tube, a magnetic force supply part located in the center of the flow path, a cooling part and a heating part on both sides, and a liquid column height measuring part. The copper pipe has an inner diameter of 7 mm, and the glass tube has an inner diameter of 6 mm; they are combined into a U-shape with tube connection joints. The cooling part is composed of an aluminum plate through which cooling water flows. sandwiching the copper pipe, and the heating part is composed of a spiral heater wound around it. For magnetic force supply, a neodymium magnet (N-40, surface magnetic flux density: 590 mT, size: $10 \times 10 \times 40$ mm) is used, and it is fixed with an acrylic plate jig to sandwich the flow path. The liquid column height is measured by placing scale tapes on the left and right glass tubes.

B. Driving Force Characteristics

To create a thermal difference at both ends of the magnet, the temperature of the cooling water flowing into the aluminum plate was fixed at 20°C, while the heater was supplied with voltages ranging from 40 to 90 V AC adjusted in 10 V increments. The relationship between the driving force and the temperature difference at both ends of the magnet is demonstrated in Fig. 5. All measurement results shown hereafter were taken when the steady state of the measuring instrument was confirmed.

C. Flow Path Temperature Distribution

Thermocouples were placed at 20 mm intervals between the cooling part and the heating part. The temperature distribution of the flow path was measured by setting the cooling water temperature to 20°C and the heating part temperature to about 100°C, and the results are shown in Fig. 6. The flow path position 0 mm is the center between the heating part and the cooling part, with the negative direction being the cooling side and the positive direction being the heating side.

A difference was observed in the temperature gradients on either side of the center point. The average slope of the temperature distribution on the high-temperature side (0–80 mm) was 0.36° C/mm. In contrast, the gradient on the low-temperature side (–80–0 mm) was 0.14° C/mm, which is gentler when compared to the high-temperature side.

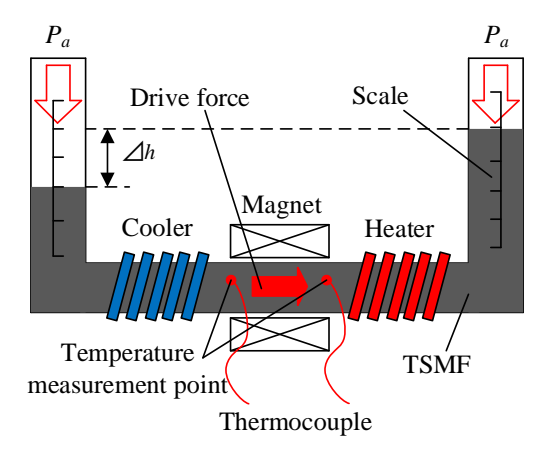


Fig. 3. Diagram of drive force measurement device.

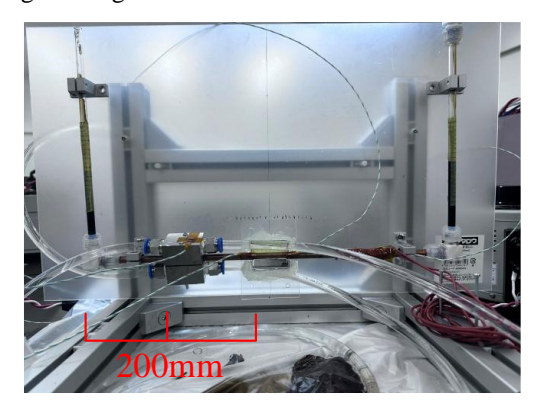


Fig. 4. The actual measurement device.

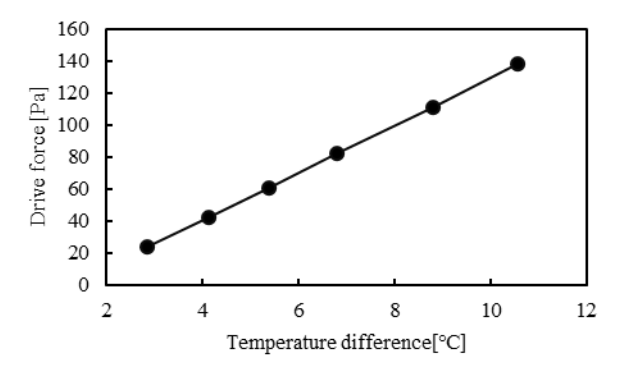


Fig. 5. Temperature difference - drive force characteristic.

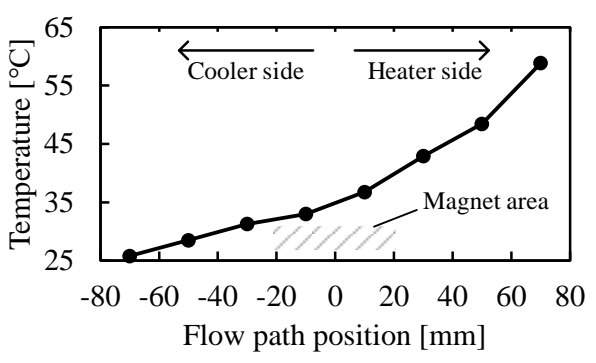


Fig. 6. Flow path temperature distribution.

This difference in gradients results from the main way heat is transferred. The steeper temperature gradient and exponential temperature distribution on the high-temperature side suggest enhanced convection driven by forces generated within the fluid. On the other hand, the relatively linear distribution on the low-temperature side suggests that heat conduction is the dominant mechanism. Consequently, it was confirmed that the temperature difference per unit distance tends to be larger on the high-temperature side.

D. Magnet Position - Driving Force Characteristics Test

Based on the experimental results in Fig. 6, the position of the magnet is also expected to be an important design parameter. Consequently, the drive force characteristics with respect to the magnet position were obtained. The cooling water temperature was set to 20°C, and the heating section temperature was set to about 100°C. The reference point for the magnet position was set at the midpoint between the heating and cooling sections. The magnet position was moved around this 0 mm reference point to -45, -30, -10, 10, 30, and 45 mm positions, and the drive force was measured at each position.

Fig. 7 shows that the driving force increases as the magnet is moved closer to the heating side from the cooling side, and the change in driving force with respect to the magnet position tends to be larger on the heating side.

This is due to a steep temperature gradient which is generated on the high-temperature side, as the results in Fig. 6 show, making it easy for a large temperature difference to occur at both ends of the magnet. Additionally, the magnet temperature was at most 30.2°C, a point where no significant thermal demagnetization occurred, and a magnetic force was being supplied. As a result, in the region where the magnet temperature does not lead to significant thermal demagnetization, it is possible to increase the driving force by bringing the magnet closer to the heating part.

IV. HEAT TRANSFER

In the previous chapter, it was found that a driving force is generated in TSMF by the magnetic force and temperature difference. In this chapter, the ability of closed-loop circulation heat transport using that driving force is verified.

A. Heat Transport Measuring Instrument

The heat transport measurement device was constructed using the configuration shown in Figure 8. This device consists of a closed-loop flow path filled with TSMF, a cooling section and a heating section, and a magnetic force supply section positioned between them. The cooling section employs cooling water flowing through aluminum plates that sandwich the pipes, similar to the driving force measurement device. The heating section incorporates a heater with a built-in thermocouple within a heat equalization plate for temperature uniformity. Copper tubing with excellent thermal conductivity was used for the sections housing the magnetic force supply unit, cooling section, and heating section. PTFE tubing was used for the remaining sections to form the closed-loop flow path. The same neodymium magnets used in the driving force measurement device were employed for the magnetic force

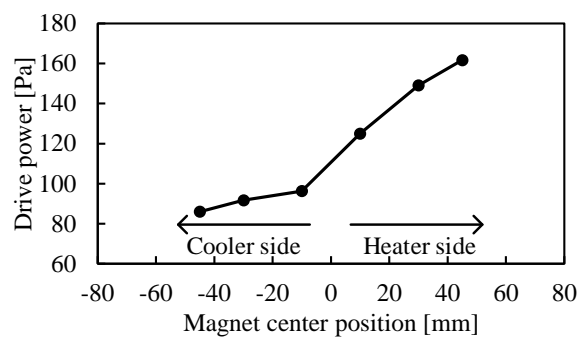


Fig. 7. Magnet position - driving force characteristic.

Table 2 Heat Transfer Measurement Instrument Components.

Equipment Role and Name	Product Name and Model	
Power supply	TEXIO PPX36-3	
Magnetic power supply	Niroku Seisakusho Neodymium magnet N-40	
Heater	Sakaguchi electric heater WALN-6	
Cooler	ORION MACHINERY RKS1503J-MV-0000	
Temperature measurement	K type Thermocouple	
Cooling plate material	Aluminum	
Soaking plate material	Brass	

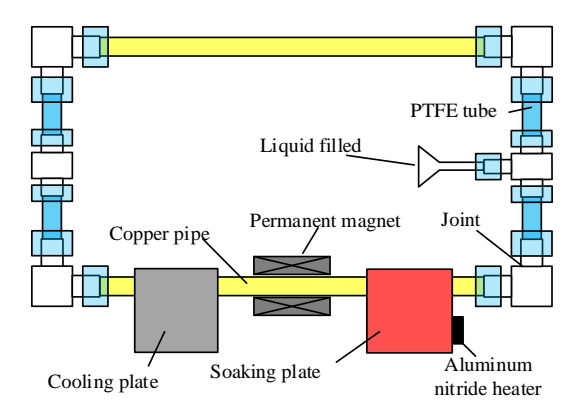


Fig. 8. Schematic diagram of the heat transfer measurement device.



Fig. 9. Thermal transport measurement device with thermal insulation treatment.

supply, positioned at the center of the heat equalization plate and the cooling plate.

The entire measuring instrument is insulated from the desk and air, allowing only TSMF to perform the heat transport process. The flow path is additionally insulated with glass wool, while a thermal insulator (Styrofoam manufactured by Dupont Styro Co.) is inserted between the joints and the desk to further enhance insulation, as shown in Fig. 9. The flow path has a total length of about 1400 mm and consists of copper pipes with an inner diameter of 7 mm and PTFE tubes with an inner diameter of 6 mm. Inside the flow path, approximately 48 mL of TSMF was filled and its temperature is monitored using a K thermocouple.

B. Heat Transfer Operation Verification

Fig. 10 shows the transition of the heater temperature with and without a magnet, with the cooling temperature fixed at 20 °C and the heater supply power fixed at 5 W. The saturation temperature differs with and without a magnet. The saturation temperature is about 96°C without a magnet and about 70°C with a magnet. This means that the TSMF is driven by the magnetic force from the magnet, and the heat from the heater is efficiently removed.

C. Relationship between Magnet Position and Heat Transfer

As explained in Chapter III, Section D, an experiment was performed to determine how the magnet's position affects heat transfer capability. Fig. 11 displays the heater temperature changes when the magnet was placed at three points—the cooling side (—40 mm), the center (0 mm), and the heating side (40 mm)—while maintaining the cooling water temperature at 20°C and setting the heater supply power to 3 W. Additionally, Table 3 shows the heater temperature at saturation and the corresponding Magnet heating end temperature in Fig. 11.

When the magnet is positioned at 40 mm on the heating side, the heater temperature is the lowest, indicating that the cooling performance increases as the magnet approaches the heating side. This result is well aligned with the finding in Fig. 6, which also shows that moving the magnet closer to the heating area increases the driving force, enabling more efficient heat transfer and consequently reducing the heater temperature.

D. Evaluation Method of Heat Transport Capacity

The heat transport capacity, which is an important characteristic for a heat transport device, is evaluated based on thermal resistance. To obtain necessary values for calculation, measurements are performed using the setup illustrated Fig. 12. As written in formula (4), the thermal resistance R_{th} [°C/W] is determined by three parameters: the inlet and temperature T_i [°C], the outlet temperature T_o [°C], and the heater power supply Q [W] [14, 18]. The inlet and outlet temperatures are defined as the average temperature of thermocouples No. 3 and No. 4 in the heating part, and thermocouples No. 1 and No. 2 in the cooling part, respectively.

$$R_{th} = \frac{T_o - T_i}{Q} \dots (4)$$

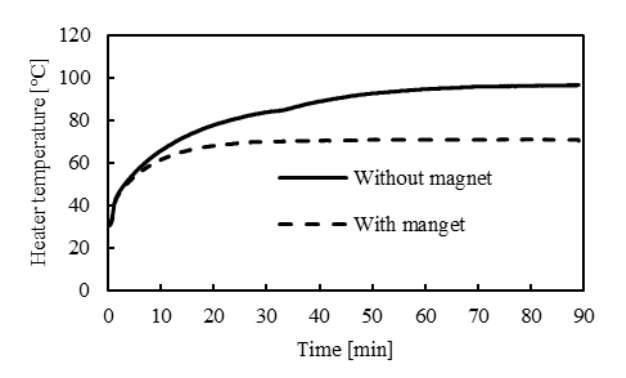


Fig. 10. Thermal transport performance test.

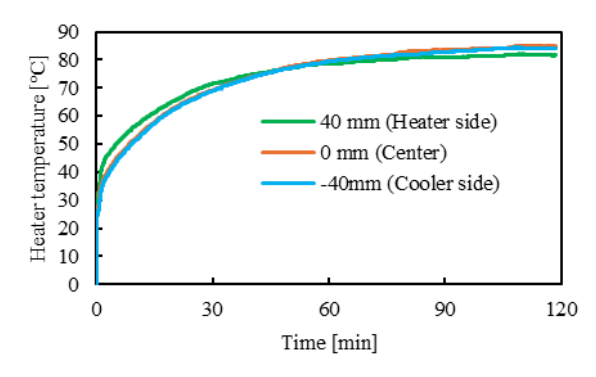


Fig. 11. Magnet position - heat transfer characteristics.

Table 3 Heater and magnet temperatures at saturation for each magnet position.

Magnet position [mm]	Saturation heater temperature [°C]	Magnet temperature [°C]
-40 (Cooler side)	84.5	28.7
0 (Center)	84.8	33.7
40 (Heater side)	81.5	38.0

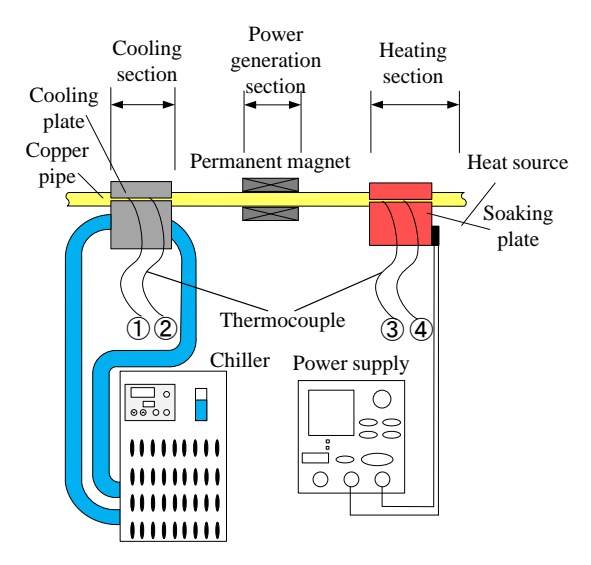


Fig. 12. Temperature measurement unit of the measuring instrument.

The flow velocity U [m/s] is calculated using the thermocouple and physical properties of the TSMF. Since the flowmeter requires calibration, the calculation was performed using only the thermocouple. The flow velocity is determined by the inlet temperature T_i [°C], the outlet temperature T_o [°C], the cross-section area A [m²] of the flow channel, the specific heat C_p [J/(kg·K)]. of TSMF, and the fluid density ρ [kg/m³].

$$U = \frac{Q}{C_p \cdot \rho A \cdot (T_o - T_i)} \qquad (5)$$

All calculations are conducted assuming that the physical properties of TSMF, except for magnetization characteristics, exhibit sufficiently small changes with respect to temperature.

E. Heat Transport Capacity

Table 4 shows the thermal resistance and flow velocity in the magnet position-heat transport characteristic test. It can be seen that when installed in the heating section, the flow velocity increases significantly and the thermal resistance decreases. Furthermore, at 0 mm and -40 mm, where the heater temperature was similar, the flow velocity and thermal resistance were also similar. Therefore, it can be said that moving closer to the heating section improves heat transport capability.

CONCLUSION

In this paper, it is concluded that the performance of a self-driven TSMF cooling device improves when permanent magnets are placed across the steep temperature gradient created by convection near a heat source. Based on this finding, design guidelines for magnet placement have been proposed. This positioning amplifies the temperature difference between the magnet's ends, which increases the magnetization inhomogeneity and leads to an increase in the driving force. As a result, the flow velocity increases, and the thermal resistance is reduced by 1.4 °C/W.

REFERENCES

- [1] IEA PVPS, "Trends in Photovoltaic Applications 2024," IEA PVPS Task 1, International Energy Agency, 2024.
- [2] D. Feldman, J. Zuboy, K. Dummit, D. Stright, M. Heine, S. Grossman, et al., "Spring 2024 Solar Industry Update. Golden," CO: National Renewable Energy Laboratory (NREL), U.S. Department of Energy, May 2024.
- [3] H. Wang, F. Blaabjerg, K. Ma and R. Wu, "Design for reliability in power electronics in renewable energy systems status and future," 4th International Conference on Power Engineering, Energy and Electrical Drives, pp. 1846-1851, 2013.
- [4] C. Rodriguez and G. A. J. Amaratunga, "Long-Lifetime Power Inverter for Photovoltaic AC Modules," in IEEE Transactions on Industrial Electronics, vol. 55, no. 7, pp. 2593-2601, 2008.
- [5] S. B. Kjaer, J. K. Pedersen and F. Blaabjerg, "A review of single-phase grid-connected inverters for photovoltaic modules," in IEEE Transactions on Industry Applications, vol. 41, no. 5, pp. 1292-1306, 2005
- [6] Shuhei Fukunaga, Yuki Nakamura, and Tsuyoshi Funaki, "Evaluation of Electrical Model Parameter Changes in SiC Power MOSFETs During

Table 4 Magnet position and flow velocity, thermal resistance.

Magnet position [mm]	Flow velocity [mm/s]	Thermal resistance [°C/W]
-40 (Cooler side)	0.975	16.3
0 (Center)	0.973	16.3
40 (Heater side)	1.07	14.9

- Power Cycling Test," IEEJ Journal of Industry Applications, vol. 13, Issue 6, pp. 731–740, 2024.
- [7] U.-M. Choi, S. Jørgensen and F. Blaabjerg, "Impact of Cooling System Capacity on Lifetime of Power Module in Adjustable Speed Drives," in IEEE Journal of Emerging and Selected Topics in Power Electronics, vol. 7, no. 3, pp. 1768-1776, 2019.
- [8] K. Ma, M. Liserre, F. Blaabjerg and T. Kerekes, "Thermal Loading and Lifetime Estimation for Power Device Considering Mission Profiles in Wind Power Converter," in IEEE Transactions on Power Electronics, vol. 30, no. 2, pp. 590-602, 2015.
- [9] Y. V. Pushpalatha, D. A. Philipps, T. F. Baumann, and D. Peftitsis, "Real-Time Discrete Electrothermal Model of Dual Active Bridge Converter for Photovoltaic Systems," in IEEE Journal of Emerging and Selected Topics in Power Electronics, vol. 12, no. 6, pp. 5493-5510, Dec. 2024.
- [10] M. Polikarpova, M. Lohtander, L. Popova, T. Musikka, R. Juntunen, P. Silventoinen, et al., "Reliability analysis of liquid cooling systems' mechanical components for 3 MVA power converter," Mechanika, vol. 19, no. 4, pp. 417–423, 2013.
- [11] D. Hill, "Why power supplies fail: A real world analysis," IEEE TV, in plenary session of APEC2016: The 30th IEEE Annual Applied Power Electronics Conference and Exposition, Long Beach, USA, Mar. 2016. [Online]. Available: https://ieeetv.ieee.org/ieeetv-specials/apec-2016david-hill-why-powersupplies-fail-a-real-world-analysis. [Accessed: Sep. 20, 2025].
- [12] R. Wrobel and R. J. McGlen, "Heat pipes in thermal management of electrical machines – A review," Thermal Science and Engineering Progress, vol. 26, 2021.
- [13] H. Baumann, P. Heinemeyer, W. Staiger, M. Töpfer, K. Unger, and D. Müller, "Optimized Cooling Systems for High-Power Semiconductor Devices," IEEE Transactions on Industrial Electronics, vol. 48, no. 2, pp. 298–306, 2001.
- [14] Z. Rong, Y. Iwamoto, Y. Ido, A. Mitani, R. Kobayashi, "Investigation of heat transfer characteristics of the self driving temperature-sensitive magnetic fluid through a nonmagnetic porous in a heating pipe," Journal of Magnetism and Magnetic Materials, vol. 590, article id. 171658, 2024.
- [15] K. Fujimoto, M. Ikegawa, H. Yamagishi, "Study on Mini-Heat Transfer Device Using Temperature-Sensitive Magnetic Fluid", Transactions of the Japan Society of Mechanical Engineers, Series B., Vol. 72, No. 723, pp. 179–185, 2006.
- [16] W. Xin-hua, J. Yu-lin, N. Yong-chao and Y. Jie, "Study on Enhanced Heat Transfer Features of Nano-magnetic Fluid Heat Pipe Under Magnetic Field," International Journal of Heat and Technology, Vol.33, No.1, pp. 137–144, 2015.
- [17] Japan Society of Mechanical Engineers, JSME Textbook Series Fluid Mechanics, pp. 29, 2018.
- [18] A. K. Mozumder, A. F. Akon, M. S. H. Chowdhury, and S. C. Banik, "Performance of Heat Pipe for Different Working Fluids and Fill Ratios," Journal of Mechanical Engineering, Vol. ME 41, No. 2, pp. 96– 102, December 2010.